

1 Emergent constraint on Arctic Ocean  
2 acidification in the twenty-first century

3 Jens Terhaar<sup>1,2,3\*</sup>, Lester Kwiatkowski<sup>1,4</sup>, Laurent Bopp<sup>1</sup>

4 <sup>1</sup> LMD/IPSL, Ecole Normale Supérieure/PSL Université, CNRS, Ecole Polytechnique, Sorbonne  
5 Université, Paris, France

6 <sup>2</sup> Climate and Environmental Physics, Physics Institute, University of Bern, Switzerland

7 <sup>3</sup> Oeschger Center for Climate Change Research, University of Bern, Switzerland

8 <sup>4</sup> LOCEAN/IPSL, Sorbonne Université, CNRS, IRD, MNHN, Paris, France

9

10

11

12

13

14 **\*Jens Terhaar**

15 **Climate and Environmental Physics, Physics Institute**

16 **University of Bern**

17 **Sidlerstrasse 5**

18 **3012 Bern**

19 **Switzerland**

20 **jens.terhaar@climate.unibe.ch**

21 The ongoing uptake of anthropogenic carbon by the ocean leads to ocean acidification, a  
22 process that results in a reduction in pH and the saturation state of biogenic calcium carbonate  
23 minerals ( $\Omega_{\text{calc/arag}}$ )<sup>1,2</sup>. Due to naturally low  $\Omega_{\text{calc/arag}}$ <sup>2,3</sup>, the Arctic Ocean is considered the most  
24 susceptible region to future acidification and associated ecosystem impacts<sup>4,5,6,7</sup>. However, the  
25 magnitude of projected twenty-first century acidification differs strongly across Earth System  
26 Models (ESMs)<sup>8</sup>. Here we identify an emergent multi-model relationship between the  
27 simulated present-day density of Arctic Ocean surface waters, used as a proxy for Arctic deep-  
28 water formation, and projections of the anthropogenic carbon inventory and coincident  
29 acidification. Applying observations of sea surface density, we constrain the end of twenty-first  
30 century Arctic Ocean anthropogenic carbon inventory to  $9.0 \pm 1.6$  Pg C and basin-averaged  $\Omega_{\text{arag}}$   
31 and  $\Omega_{\text{calc}}$  to  $0.76 \pm 0.06$  and  $1.19 \pm 0.09$  respectively, under the RCP 8.5 climate scenario. Our  
32 results indicate greater regional anthropogenic carbon storage and ocean acidification than  
33 previously projected<sup>3,8</sup> and increase the probability that large parts of the mesopelagic Arctic  
34 Ocean will be undersaturated with respect to calcite by the end of the century. This increased  
35 rate of Arctic Ocean acidification combined with rapidly changing physical and biogeochemical  
36 Arctic conditions<sup>9,10,11</sup>, is likely to exacerbate the impact of climate change on vulnerable Arctic  
37 marine ecosystems.

38

39

40

41 While the uptake of atmospheric carbon by the ocean mitigates climate change, it also  
42 dramatically influences marine chemistry, decreasing pH and carbonate ion concentrations  
43  $[\text{CO}_3^{2-}]$  and increasing concentrations of aqueous carbon dioxide and bicarbonate ions  $[\text{HCO}_3^-]$ <sup>1,2</sup>.  
44 These changes in seawater chemistry, collectively known as ocean acidification, have been shown  
45 to negatively impact wide-ranging marine organisms including molluscs, crustaceans,  
46 echinoderms, cnidarians and teleost fish<sup>4,5,6,7</sup>. Calcifying marine organisms are particularly  
47 sensitive to ocean acidification, which can impair their growth, reproduction and survival<sup>2,4,12</sup>.  
48 The thermodynamic stability of calcium carbonate is described by the calcium carbonate  
49 saturation state ( $\Omega = [\text{Ca}^{2+}][\text{CO}_3^{2-}]/K_{sp}$ ), with  $K_{sp}$  representing the relevant  $\text{CaCO}_3$  solubility  
50 product, and  $\Omega_{\text{calc}}$  and  $\Omega_{\text{arag}}$  representing the saturation state of the stable calcite and metastable  
51 aragonite mineral forms, respectively. Ocean acidification acts to reduce  $\Omega$  by reducing  
52 carbonate ion concentrations. Studies have shown that as  $\Omega$  decreases, calcification rates at both  
53 the organism<sup>12,13,14</sup> and community-level<sup>15</sup> typically decline. In addition, the corrosion of pure  
54 mineral forms is actively promoted under exposure to undersaturated conditions ( $\Omega < 1$ ).

55

56 The Arctic represents the global region projected to experience the most severe climate change,  
57 with polar amplification causing a projected end-of-century surface temperature increase of up  
58 to  $8.3 \pm 1.9$  °C<sup>10</sup> and loss of summer sea-ice<sup>11</sup>. The same is true for the Arctic Ocean, where low  
59 temperatures and consequently the high solubility of  $\text{CO}_2$ , result in naturally low pH and  $\Omega$ <sup>2,3</sup>.  
60 Given this natural state and the amplifying effect of climate change<sup>16</sup>, the Arctic Ocean is

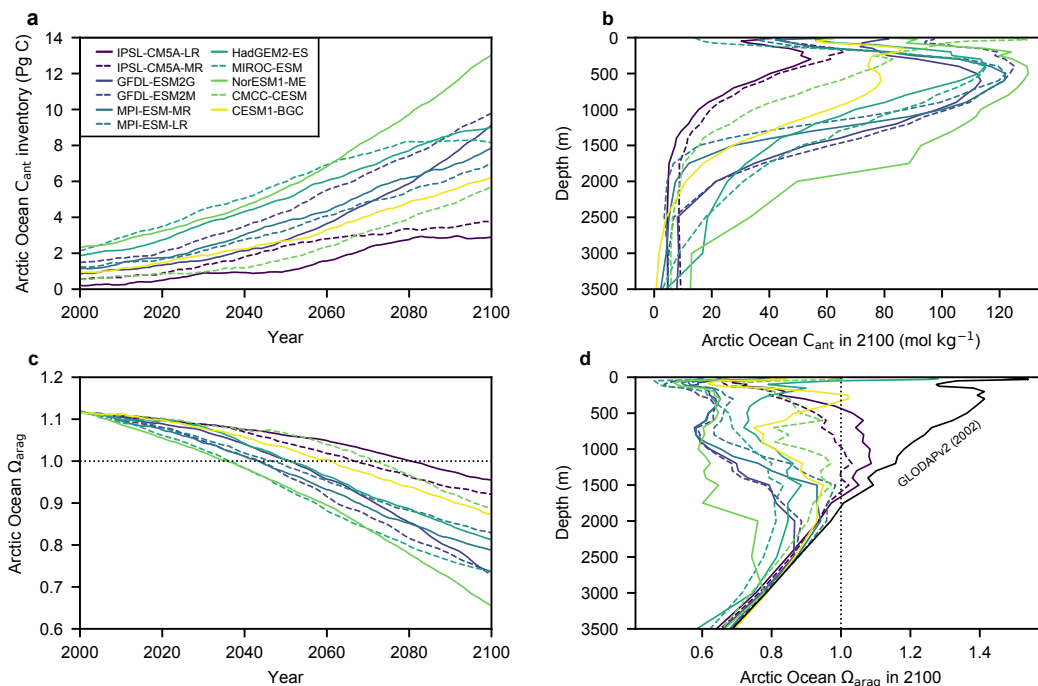
61 projected to experience the lowest pH and  $\Omega$  conditions in the coming decades<sup>3</sup>, as well as  
62 dramatic changes in the temporal variability of marine chemistry<sup>9</sup>.

63

64 Projections by ESMs under the high-emissions Representative Concentration Pathway 8.5  
65 (RCP8.5)<sup>17</sup> suggest that the entire Arctic Ocean will be undersaturated with respect to aragonite  
66 ( $\Omega_{\text{arag}} < 1$ ) by the end of the twenty-first century (Fig. 1), while basin-wide calcite undersaturation  
67 ( $\Omega_{\text{calc}} < 1$ ) is not expected to occur this century<sup>3,8,18</sup> (Extended Data Figure 1). Projected changes  
68 in ocean chemistry are predominantly confined to the upper 2500 m of the water column, with  
69 large model uncertainties persisting with regard to the end-of-century anthropogenic carbon  
70 inventory (2.9-13.0 Pg C)<sup>19</sup>, and the associated average  $\Omega_{\text{arag}}$  (0.66-0.95) and  $\Omega_{\text{calc}}$  (1.02-1.49)<sup>8</sup>.  
71 Although projection uncertainties are limited in the surface ocean<sup>20</sup>, they are highly pronounced  
72 at depth (Fig. 1 and Extended Data Figure 1) and complicate assessments of likely impacts on  
73 vulnerable marine ecosystems<sup>7</sup>.

74





75

76 **Fig. 1. Projections of Arctic Ocean anthropogenic carbon and aragonite saturation state.** a, ESM  
 77 projections of the twenty-first century Arctic Ocean anthropogenic carbon ( $C_{ant}$ ) inventory and c, basin-  
 78 averaged  $\Omega_{arag}$ . Vertical profiles of b, basin-averaged anthropogenic carbon and d,  $\Omega_{arag}$  in 2100 for the 11  
 79 ESMs. The GLODAPv2<sup>24</sup> observational profile of  $\Omega_{arag}$  for 2002 is marked as a black line in d. Arctic Ocean  
 80 boundaries are the Fram Strait, the Barents Sea Opening, the Bering Strait and the Canadian Arctic  
 81 Archipelago.

82

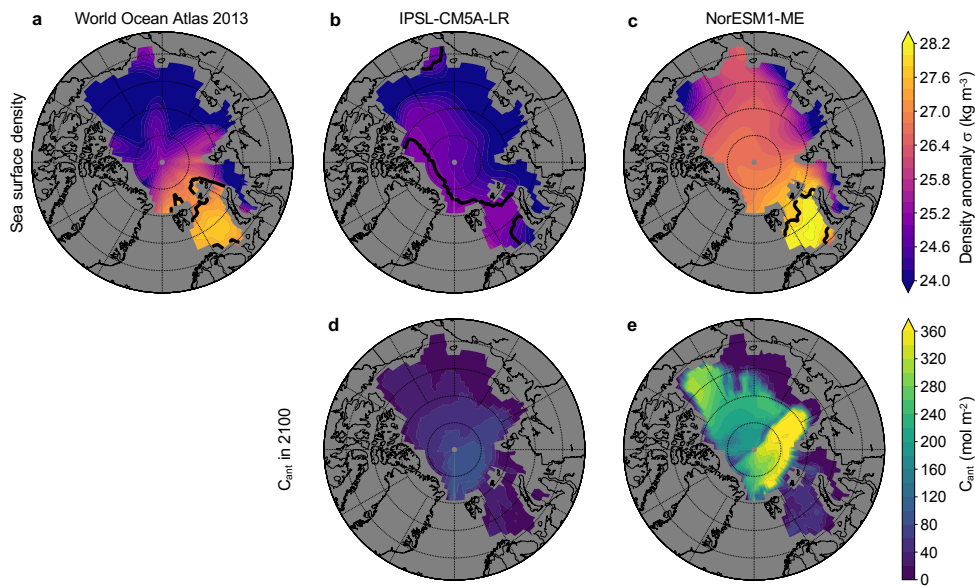
83 To reduce Arctic Ocean projection uncertainties associated with the anthropogenic carbon  
 84 inventory and concurrent acidification, here we utilise the recent approach of emergent  
 85 constraints<sup>11,21,22,23</sup>. In order to constrain future ESM projection uncertainties, emergent  
 86 constraints relate long-timescale climate sensitivities and impacts to observable properties, such  
 87 as short-timescale climate variability or trends, across ESM ensembles. Emergent constraints

88 have previously been used to reduce the uncertainty, amongst other climate projections,  
89 associated with Arctic summer sea ice<sup>11</sup>, equilibrium climate sensitivity<sup>22</sup> and impacts on marine  
90 primary production<sup>21</sup>.

91

92 Here we show that across an ensemble of 11 ESMs (Table S1) there is a consistent relationship  
93 between present-day Arctic Ocean maximum sea surface water density, the projected end-of-  
94 century Arctic Ocean anthropogenic carbon inventory and the extent of ocean acidification under  
95 RCP8.5 (Fig. 2, 3). All models performed simulations as part of the Coupled Model  
96 Intercomparison Project Phase 5 (CMIP5). Present-day (1986-2005) maximum sea surface density  
97 was calculated, for each model, as the mean of the 95<sup>th</sup> percentile of monthly surface water  
98 densities in the Arctic. Across all models, these maximum density waters are primarily located in  
99 the Barents Sea (Extended Data Figure 2). The anthropogenic carbon inventory was calculated as  
100 the difference in integrated Arctic Ocean dissolved inorganic carbon between RCP8.5 simulations  
101 and the respective pre-industrial control simulation of each model. While projections of variables  
102 associated with ocean acidification ( $\Omega_{\text{calc/arag}}$ , pH and  $p\text{CO}_2$ ) were calculated from model outputs  
103 of total alkalinity, dissolved inorganic carbon, temperature, salinity, total dissolved inorganic  
104 phosphorus and silicon and bias-corrected using GLODAPv2<sup>24</sup> (see Methods).

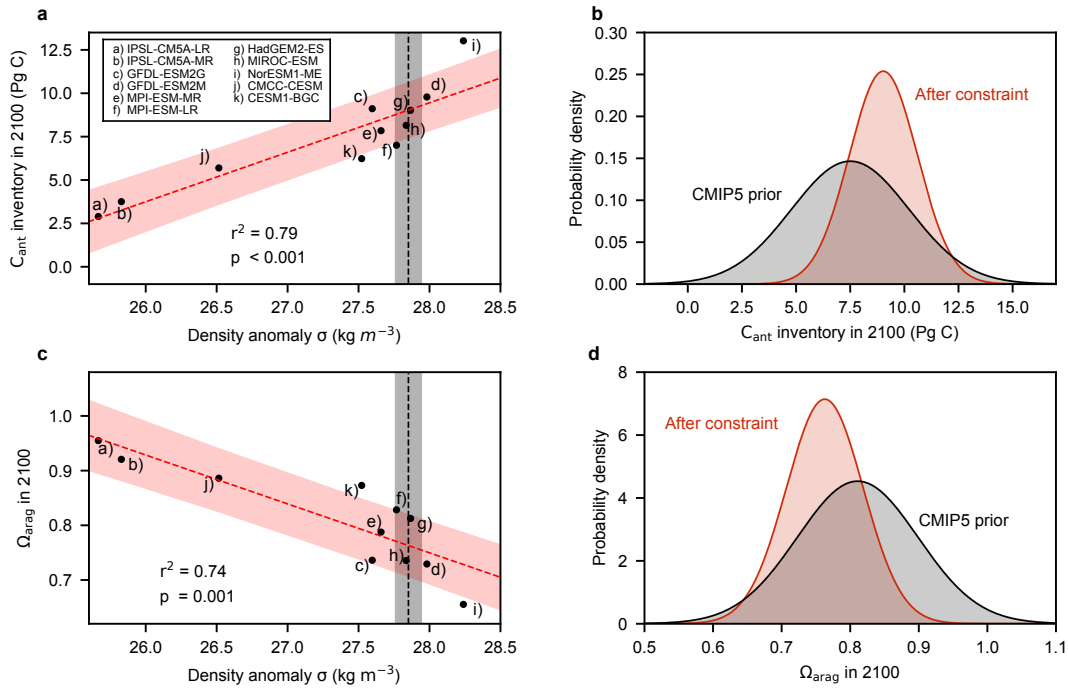
105



106

107 **Fig. 2. Arctic Ocean surface water density and the anthropogenic carbon inventory.** a, Present-  
 108 day annual-mean sea surface density from World Ocean Atlas 2013<sup>25</sup> and the b, IPSL-CM5A-LR  
 109 and c, NorESM1-ME models. Contours delineate regions that contribute to the maximum surface  
 110 density as defined by the 95<sup>th</sup> percentile densities. Vertically integrated anthropogenic carbon  
 111 ( $C_{ant}$ ) projections in 2100 for the d, IPSL-CM5A-LR and e, NorESM1-ME models. IPSL-CM5A-LR  
 112 represents the ensemble minimum for both present-day maximum sea surface density (1025.67  
 113  $\text{kg m}^{-3}$ ) and projected  $C_{ant}$  inventory in 2100 (2.9 Pg C), while NorESM1-ME is the ensemble  
 114 maximum (1028.24  $\text{kg m}^{-3}$  and 13.0 Pg C). The maximum sea surface density from WOA 2013 is  
 115 1027.85  $\text{kg m}^{-3}$

116



117

118 **Fig. 3. Emergent constraints on the projected anthropogenic carbon inventory and**  
 119 **acidification. a,** The projected Arctic Ocean anthropogenic carbon inventory and **c,** basin-  
 120 averaged  $\Omega_{arag}$  in 2100 against present-day maximum sea surface density (95<sup>th</sup> percentile waters)  
 121 for the ESM ensemble (black dots). Linear regression fits (red dashed lines) and the associated  
 122 68 % prediction intervals are shown, as are data-based estimates of present-day maximum sea  
 123 surface density (black dashed lines) with the associated standard deviation (black shaded area).  
 124 Probability density functions for the end-of-century **b,** Arctic Ocean anthropogenic carbon  
 125 inventory and **d,** basin-averaged  $\Omega_{arag}$ , before (black) and after (red) the emergent constraint is  
 126 applied.

127

128

129 ESMS such as IPSL-CM5A-LR, which simulate lower than observed present-day Arctic Ocean  
130 maximum surface densities, a proxy for Arctic deep-water formation (Extended Data Figure 3),  
131 typically project lower end-of-century anthropogenic carbon inventories under RCP8.5 than  
132 models such as NorESM1-ME, which simulate higher densities (Fig. 2). This emergent relationship  
133 across the ESM ensemble is consistent at the scale of the Arctic Ocean basin, with present-day  
134 maximum surface density exhibiting a strong relationship with end-of-century depth integrated  
135 anthropogenic carbon inventories ( $r^2=0.79$ ,  $P < 0.001$ ; Fig. 3). Given the dominance of  
136 anthropogenic carbon uptake in driving ocean acidification (Extended Data Figure 4), models with  
137 higher maximum sea surface density also exhibit stronger twenty-first century reductions in  
138 basin-average  $\Omega_{\text{arag}}$  ( $r^2=0.74$ ,  $P = 0.001$ ; Fig. 3),  $\Omega_{\text{calc}}$  ( $r^2=0.74$ ,  $P = 0.001$ ; Extended Data Figure 1)  
139 and pH ( $r^2=0.77$ ,  $P < 0.001$ ; Extended Data Figure 1). Observations of sea surface density<sup>25</sup> were  
140 then used in combination with these multi-model relationships, to provide emergent constraints  
141 on projections of Arctic Ocean anthropogenic carbon storage, and concomitant acidification.  
142 Potential alternative constraints, such as present-day seasonal sea ice extent, were found to be  
143 non-indicative of future Arctic Ocean anthropogenic carbon and acidification across the ESM  
144 ensemble (Extended Data Figure 3).

145

146 Our emergent constraint increases projections of the end-of-century Arctic Ocean anthropogenic  
147 carbon inventory from  $7.5 \pm 2.7$  Pg C (CMIP5 multi-model mean) to  $9.0 \pm 1.6$  Pg C, with a 41 %  
148 reduction in uncertainty (Fig. 3). Similarly, average end-of-century  $\Omega_{\text{arag}}$  and  $\Omega_{\text{calc}}$  are reduced  
149 from  $0.81 \pm 0.09$  to  $0.76 \pm 0.06$  and from  $1.27 \pm 0.14$  to  $1.19 \pm 0.09$ , respectively (Fig. 3, Extended

150 Data Figure 1). As such, the low bias of maximum sea surface density in 8 of 11 ESMs is indicative  
151 of an underestimation of projected anthropogenic carbon storage and therefore future Arctic  
152 Ocean acidification in the CMIP5 multi-model mean.

153

154 The mechanisms underpinning the relationship between maximum surface densities and  
155 anthropogenic carbon uptake are intrinsically related to Arctic Ocean circulation and dynamics.  
156 The majority of intermediate and deep Arctic waters and the anthropogenic carbon they carry  
157 are of Atlantic origin<sup>26,27</sup>. The dominant net influx of anthropogenic carbon from the Atlantic into  
158 the Arctic Ocean is through the Barents Sea Opening, as indicated by both data-based estimates<sup>28</sup>  
159 ( $41 \pm 8 \text{ Tg C yr}^{-1}$ ) and ocean carbon cycle models (21-48  $\text{Tg C yr}^{-1}$ ; Table S2). This inflowing water  
160 is seasonally cooled in the Barents Sea via surface heat exchange and enriched in salinity via brine  
161 rejection during the formation of sea ice<sup>29,30</sup>. Consequently, during winter, seawater density  
162 increases and water masses sink into the interior Arctic Ocean, mainly via the St Anna Trough,  
163 where they supply most intermediate and deep waters<sup>26,27</sup>. As such, the present-day ability of  
164 ESMs to simulate the maximum surface densities that occur in the Barents Sea, is highly indicative  
165 of their capacity to transport future anthropogenic carbon into the Arctic interior.

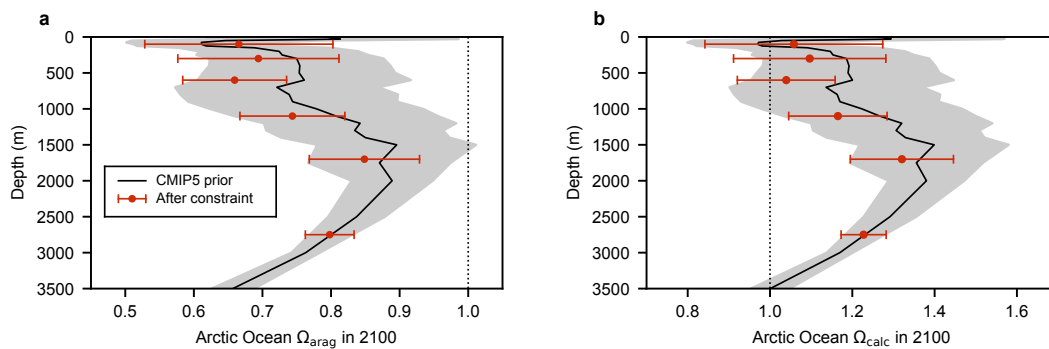
166

167 These mechanisms were further explored in historical (1870-2012) simulations of an ocean-only  
168 carbon-cycle model (NEMO-PISCES), performed at three spatial resolutions<sup>19</sup>. These simulations  
169 confirm the importance of Atlantic waters that flow into the Barents Sea, in determining net  
170 changes in the Arctic Ocean anthropogenic carbon inventory (Table S2). They further show that

171 across model spatial resolutions there is a strong positive relationship ( $r^2=0.98$ ,  $P = 0.08$ ; Fig. S1)  
 172 between maximum surface density and the historical change in Arctic Ocean anthropogenic  
 173 carbon inventory (Fig. S2). One of the principal drivers of the CMIP5 emergent relationship  
 174 therefore appears to be variable ESM resolution and associated difficulties in resolving the  
 175 transport of anthropogenic carbon into the Arctic basin at low resolutions<sup>19</sup>. Indeed, CMIP5 ESMs  
 176 with higher Arctic Ocean resolution typically project greater end-of-century anthropogenic  
 177 carbon inventories ( $r^2=0.44$ ,  $P = 0.03$ ; Extended Data Figure 3).

178

179



180

181 **Fig. 4. Constrained end-of century Arctic Ocean vertical profiles of  $\Omega_{\text{calc/arag}}$ .** Multi-model mean  
 182 vertical profiles of basin-averaged **a**,  $\Omega_{\text{arag}}$  and **b**,  $\Omega_{\text{calc}}$  in 2100 (black lines) with the associated  
 183 standard deviation ( $n=11$ ; grey shading). Constrained mean estimates of  $\Omega_{\text{arag}}$  and  $\Omega_{\text{calc}}$  (red dots)  
 184 are shown for six different depth layers (0-200 m, 200-400 m, 400-800 m, 800-1400 m, 1400-  
 185 2000 m, 2000 m - bottom). The constrained estimates are shown at the mid-point of each layer,  
 186 with error bars representing  $\pm$  one standard deviation.

187

188 Extending the emergent constraint approach from the entire Arctic basin to multiple vertical  
189 depth integrals, we reduce uncertainties associated with projections of changing vertical profiles  
190 of  $\Omega_{\text{calc/arag}}$  (Fig. 4, Extended Data Figures 5, 6), pH and  $p\text{CO}_2$  (Extended Data Figures 7, 8). Basin-  
191 wide emergent constraints on twenty-first century acidification are shown to be predominantly  
192 driven by subsurface waters between 400 and 1400 m, with the strongest multi-model  
193 relationship between present-day maximum surface density and end-of-century  $\Omega_{\text{calc/arag}}$  found  
194 between 400 and 800 m ( $r^2 = 0.84$ ,  $P < 0.001$ ; Extended Data Figures 5, 6). In these mesopelagic  
195 waters, end-of-century  $\Omega_{\text{arag}}$  is reduced from a CMIP5 multi-model mean of  $0.75 \pm 0.15$  to  $0.66 \pm$   
196  $0.08$ , with end-of-century  $\Omega_{\text{calc}}$  reduced from  $1.18 \pm 0.23$  to  $1.04 \pm 0.12$ . A consequence of our  
197 constrained vertical profiles of marine chemistry is that the lowest average end-of-century  
198  $\Omega_{\text{calc/arag}}$  will likely not occur in Arctic Ocean surface waters, as previously expected<sup>3,8</sup>, but  
199 between 400-800 m (Fig. 4). In these mesopelagic waters, the probability of end-of-century  $\Omega_{\text{calc}}$   
200  $< 1$  and  $\Omega_{\text{arag}} < 0.75$  is increased from 23% and 51% respectively in the CMIP5 prior to 37% and  
201 88% respectively after the constraint is applied (Extended Data Table 1).

202

203 In the upper Arctic Ocean (0-200 m), present-day maximum surface density exhibits limited  
204 relationship with end-of-century  $\Omega_{\text{calc/arag}}$  across the models (Extended Data Figures 5, 6) and  
205 emergent constraints offer no reduction in projection uncertainties (Fig. 4). This is to be expected  
206 in waters where deep-water formation has little impact on marine chemistry. Similarly, below  
207 2000 m where there is limited change in the anthropogenic carbon inventory and associated



208 marine chemistry this century (Fig. 1, Extended Data Figure 1), there is no relationship between  
209 present-day maximum surface density and end-of-century  $\Omega_{\text{calc/arag}}$  (Extended Data Figures 5, 6).

210

211 The constrained estimates of greater twenty-first century Arctic Ocean acidification presented  
212 here, have major implications for sensitive Arctic marine ecosystems already exposed to multiple  
213 climatic stressors. Enhanced subsurface acidification is likely to have negative consequences on  
214 organisms that both permanently inhabit the mesopelagic and those that utilise it as part of  
215 seasonal or diel vertical migrations<sup>31</sup>. The suitable habitat available to keystone species such as  
216 the aragonitic pteropod *Limacina helicina* is likely to decline to a greater extent than previously  
217 anticipated given its sensitivity to  $\Omega_{\text{arag}}$ <sup>32</sup>, with negative consequences for dependent pelagic food  
218 webs<sup>33,34,35</sup>. Meanwhile, undersaturation with respect to calcite is likely to have major  
219 consequences for calcite forming Arctic coccolithophores<sup>36</sup> and foraminifera<sup>37</sup>. Finally, our  
220 estimates of higher end-of century Arctic Ocean  $p\text{CO}_2$ , which increases from  $1070 \pm 239 \mu\text{atm}$  at  
221 depths of 400-800 m to  $1216 \pm 121 \mu\text{atm}$  under the constraint (Extended Data Figure 8), is likely  
222 to negatively affect the growth, survival<sup>38</sup> and behaviour<sup>39,40</sup> of ecologically important fish such  
223 as polar cod.

224

225 **References**

- 226 1. Haugan, P. M. & Drange, H. Effects of CO<sub>2</sub> on the ocean environment. *Energy Convers.*  
227 *Mgmt* **37**, 1019–1022 (1996).
- 228 2. Orr, J. C. et al. Anthropogenic ocean acidification over the twenty-first century and its  
229 impact on calcifying organisms. *Nature* **437**, 681–686 (2005).
- 230 3. Steinacher, M., Joos, F., Frolicher, T. L., Plattner, G. K. & Doney, S. C. Imminent ocean  
231 acidification in the Arctic projected with the NCAR global coupled carbon cycle-climate model.  
232 *Biogeosciences* **6**, 515–533 (2009).
- 233 4. Fabry, V. J., McClintock, J. B., Mathis, J. T. & Grebmeier, J. M. Ocean acidification at high  
234 latitudes: The bellweather. *Oceanography* **22**, 160–171 (2009).
- 235 5. Gattuso, J.-P. & Hansson, L. *Ocean Acidification* (Oxford Univ. Press, 2011).
- 236 6. Riebesell U, Gattuso JP, Thingstad TF, Middelburg JJ. Preface “Arctic ocean acidification:  
237 pelagic ecosystem and biogeochemical responses during a mesocosm study”. *Biogeosciences*  
238 **10**(8), 5619–5626 (2013).
- 239 7. AMAP, 2018. AMAP Assessment 2018: Arctic Ocean Acidification. Arctic Monitoring and  
240 Assessment Programme (AMAP), Tromsø, Norway. vi+187pp
- 241 8. Steiner, N. S., Christian, J. R., Six, K. D., Yamamoto, A., & Yamamoto-Kawai, M. Future  
242 ocean acidification in the Canada Basin and surrounding Arctic Ocean from CMIP5 earth system  
243 models. *Journal of Geophysical Research: Oceans* **119**(1), 332–347 (2014).

- 244 9. Kwiatkowski, L. & Orr, J.C. Diverging seasonal extremes for ocean acidification during  
245 the twenty-first century. *Nature Climate Change* **8**(2), 141 (2018)
- 246 10. Collins, M. et al. in *Climate Change 2013: The Physical Science Basis* (eds Stocker, T. F. et  
247 al.) 1029–1136 (IPCC, Cambridge Univ. Press, 2013).
- 248 11. Boé, J., Hall, A. & Qu, X. September sea ice cover in the Arctic Ocean projected to vanish  
249 by 2100. *Nature Geosci.* **2**, 341–343 (2009).
- 250 12. Kroeker, K. J., Kordas, R. L., Crim, R. N. & Singh, G. G. Meta-analysis reveals negative yet  
251 variable effects of ocean acidification on marine organisms. *Ecol. Lett.* **13**, 1419–1434 (2010).
- 252 13. Langdon, C. & Atkinson, M. Effect of elevated  $p\text{CO}_2$  on photosynthesis and calcification  
253 of corals and interactions with seasonal change in temperature/irradiance and nutrient  
254 enrichment. *J. Geophys. Res.* **110**, C09S07 (2005).
- 255 14. Bednaršek, N., Tarling, G. A., Bakker, D. C., Fielding, S. & Feely, R. A. Dissolution  
256 dominating calcification process in polar pteropods close to the point of aragonite  
257 undersaturation. *PLoS ONE* **9**(10), e109183 (2014).
- 258 15. Albright, R. et al. Reversal of ocean acidification enhances net coral reef calcification.  
259 *Nature* **531**, 362–365 (2016).
- 260 16. Yamamoto-Kawai, M., McLaughlin, F. A., Carmack, E. C., Nishino, S. & Shimada, K.  
261 Aragonite undersaturation in the Arctic Ocean: Effects of ocean acidification and sea ice melt.  
262 *Science* **326**, 1098–1100 (2009).

- 263 17. Riahi, K. et al. RCP 8.5—A scenario of comparatively high greenhouse gas emissions.  
264 *Clim. Change* **109**, 33–57 (2011).
- 265 18. Feely, R. A., Doney, S. C. & Cooley, S. R. Ocean acidification: Present conditions and future  
266 changes in a high-CO<sub>2</sub> world. *Oceanography* **22**, 36–47 (2009).
- 267 19. Terhaar, J., Orr, J. C., Gehlen, M., Ethé, C., and Bopp, L. Model constraints on the  
268 anthropogenic carbon budget of the Arctic Ocean. *Biogeosciences* **16**, 2343–2367 (2019).
- 269 20. Frolicher, T. L., Rodgers, K., Stock, C. & Cheung, W. W. L. Sources of uncertainties in 21st  
270 century projections of potential ocean ecosystem stressors. *Global Biogeochem. Cycles* **30**,  
271 1224–1243 (2016).
- 272 21. Kwiatkowski, L. et al. Emergent constraints on projections of declining primary production  
273 in the tropical oceans. *Nat. Clim. Chang.* **7**, 355–358 (2017).
- 274 22. Cox, P. et al. Sensitivity of tropical carbon to climate change constrained by carbon  
275 dioxide variability. *Nature* **494**, 341–344 (2013)
- 276 23. Eyring, V. et al. Taking climate model evaluation to the next level. *Nat. Clim. Chang.* **9**,  
277 102–110 (2019).
- 278 24. Lauvset, S. K. et al. A new global interior ocean mapped climatology: the 1°×1° GLODAP  
279 version 2. *Earth Syst. Sci. Data* **8**, 325–340 (2016).
- 280 25. Boyer, T. P. et al. *World Ocean Database 2013* (Silver Spring, accessed March 2019).
- 281 26. Rudels, B., Jones, E. P., Anderson, L. G., & Kattner, G. On the intermediate depth waters

282 of the Arctic Ocean. *The polar oceans and their role in shaping the global environment*, **85**, 33-46  
283 (1994).

284 27. Rudels, B., Muench, R. D., Gunn, J., Schauer, U., & Friedrich, H. J. Evolution of the Arctic  
285 Ocean boundary current north of the Siberian shelves. *J. Marine Syst.*, **25**(1) . (2001). 77-99.

286 28. Jeansson, E. et al. The Nordic Seas carbon budget: Sources, sinks, and uncertainties.  
287 *Global Biogeochem, Cy.*, **25**(4). (2011)

288 29. Midttun, Lars. "Formation of dense bottom water in the Barents Sea." *Deep Sea Res.*  
289 **32.10**, 1233-1241 (1985)

290 30. Smedsrud, L. H. et al. The role of the Barents Sea in the Arctic climate system. *Rev.*  
291 *Geophys.* **51**, 415–449 (2013).

292 31. Berge, J. et al. In the dark: A review of ecosystem processes during polar night. *Prog.*  
293 *Oceanogr.* **139**, 258–271 (2015).

294 32. Comeau, S., Jeffree, R., Teyssie, J. L. & Gattuso, J. P. Response of the Arctic pteropod  
295 *Limacina helicina* to projected future environmental conditions. *PLoS ONE* **5**, e11362 (2010).

296 33. Hunt, B. P. V. et al. Pteropods in Southern Ocean ecosystems. *Prog. Oceanogr.* **78**, 193–  
297 221 (2008).

298 34. Armstrong, J. L. et al. Distribution, size, and interannual, seasonal and diel food habits of  
299 northern Gulf of Alaska juvenile pink salmon, *Oncorhynchus gorbuscha*. *Deep-Sea Res. Pt. II* **52**,  
300 247–265 (2005).

- 301 35. Karnovsky, N. J., Hobson, K. A., Iverson, S., & Hunt Jr, G. L. Seasonal changes in diets of  
302 seabirds in the North Water Polynya: a multiple-indicator approach. *Mar. Ecol. Prog. Ser.*, **357**,  
303 291–299 (2008).
- 304 36. Kottmeier, D. M., Rokitta, S. D., & Rost, B. H<sup>+</sup>-driven increase in CO<sub>2</sub> uptake and decrease  
305 in HCO<sub>3</sub><sup>-</sup> uptake explain coccolithophores' acclimation responses to ocean acidification. *Limnol.*  
306 *Oceanogr.* **61**, 2045–2057 (2016)
- 307 37. Davis, C. V. et al. Ocean acidification compromises a planktic calcifier with implications for  
308 global carbon cycling. *Sci. Rep.* **7**, 2225 (2017)
- 309 38. Frommel, A. Y. et al. Severe tissue damage in Atlantic cod larvae under increasing ocean  
310 acidification. *Nature Clim. Change* **2**, 42–46 (2012).
- 311 39. Schmidt, M. et al. Differences in neurochemical profiles of two gadid species under ocean  
312 warming and acidification. *Front. Zool.* **14**, 49 (2017).
- 313 40. Kunz, K. et al. Aerobic capacities and swimming performance of polar cod (*Boreogadus*  
314 *saida*; lepechin) under ocean acidification and warming conditions. *J. Exp. Biol.* **221** (2018)

315

## 316 **Methods**

317

### 318 **Earth System Models**

319 In the ensemble of 11 Coupled Model Intercomparison Project Phase 5 (CMIP5) ESMs (Table S1)  
320 utilised, all included coupled ocean biogeochemistry schemes and have been extensively applied  
321 within the context of both climate and ocean biogeochemical projections<sup>8,9,21</sup>. A single ensemble  
322 member was utilised for each ESM. Prognostic annual model output fields of dissolved inorganic  
323 carbon, total alkalinity, dissolved inorganic phosphorus and silicon, temperature, and salinity  
324 were taken across all vertical depth levels in the Arctic Ocean, limited by the Fram Strait, the  
325 Barents Sea Opening, the Bering Strait and the Canadian Arctic Archipelago<sup>19,41</sup>. Monthly sea  
326 surface density outputs were taken over the same domain. All output fields were regridded on a  
327 regular 1°×1° grid to facilitate multi-model analysis.

328 The anthropogenic carbon inventory was calculated as the difference between dissolved  
329 inorganic carbon in historical (1850-2005) simulations merged with RCP8.5 (2006-2100) and the  
330 concurrent pre-industrial control (piControl) simulations. As such, any model drift in deep-ocean  
331 dissolved inorganic carbon was directly accounted for. Across all models, the simulated present-  
332 day (2005) Arctic Ocean anthropogenic carbon inventory (0.2-2.4 Pg C) is below the data-based  
333 estimate of 2.5-3.3 Pg C<sup>42</sup>.

334 All carbonate chemistry variables were calculated offline from dissolved inorganic carbon, total  
335 alkalinity, temperature, salinity and where available, dissolved inorganic phosphorus and silicon,  
336 over 1850-2100 using mocsy2.0<sup>43</sup> and the equilibrium constants recommended for best

337 practices<sup>44</sup>. To account for carbonate chemistry biases in the present-day mean state of the  
338 ESMs<sup>8</sup>, model anomalies of all input variables relative to 2002 were combined with the data-  
339 based GLODAPv2 observational product<sup>24</sup> which is normalised to the year 2002. Model anomalies  
340 were corrected for potential model drift using concurrent piControl simulations. All grid cells with  
341 GLODAPv2 observational coverage (~65 % of Arctic Ocean volume) were utilised. Basin-wide  
342 averages of  $\Omega_{\text{arag}}$ ,  $\Omega_{\text{calc}}$ , pH and  $p\text{CO}_2$  were weighted based on grid cell volumes.

343 The Arctic Ocean present-day maximum sea surface density was calculated for each ESM from  
344 1986-2005 monthly sea surface density climatologies, constructed from temperature and salinity  
345 outputs. Maximum present-day sea surface density was defined as the mean density of the  
346 densest 5 % of Arctic surface waters (95<sup>th</sup> percentile waters) throughout the climatological year.  
347 Maximum present-day sea surface density consistently occurs in the Barents Sea, across both  
348 observations and the ESM ensemble. Given the importance of the Barents Sea in supplying  
349 intermediate and deep Arctic waters<sup>26,27,29,30</sup>, maximum sea surface density, as defined, is  
350 indicative of the bowl of ventilated Arctic waters. Across all models, the volume of Arctic Ocean  
351 waters that are lighter than the maximum sea surface density increases with the maximum sea  
352 surface density ( $r^2 = 0.59$ ,  $P=0.006$ ; Extended Data Figure 3).

353 In addition to sea surface density, alternative potential constraints on the projected Arctic Ocean  
354 anthropogenic carbon inventory and associated acidification were assessed. The representation  
355 of Arctic sea ice extent<sup>45</sup> and intermediate North Atlantic water masses<sup>46</sup> varies substantially  
356 across the CMIP5 ensemble. However, both present-day sea-ice extent (Extended Data Figure 3)



357 and the properties of North Atlantic water masses were found to be non-indicative of projected  
358 Arctic Ocean carbon uptake and associated acidification across the model ensemble.

359 An assessment of the potential for model internal variability to influence the Arctic Ocean  
360 emergent constraint approach is provided in the supplementary material. Utilising four ensemble  
361 members of the IPSL-CM5A-LR model, the internal variability of present-day sea surface density  
362 and projected anthropogenic carbon inventory is shown to be highly limited compared to the  
363 differences across the CMIP5 models (Extended Data Figure 9).

364

### 365 **Ocean-only simulations**

366 Hindcast ocean-biogeochemical simulations of the NEMO-PISCES model<sup>47</sup> that have been  
367 previously published<sup>19</sup> are used in this study to explore the mechanisms behind the identified  
368 Arctic Ocean emergent constraint. The model is run at a nominal resolution of 0.5° from 1870 to  
369 1958 and at three different nominal horizontal resolutions from 1958 to 2012: 2° (ORCA2), 0.5°  
370 (ORCA05), and 0.25° (ORCA025). All three model configurations are forced with the DRAKKAR  
371 historical reanalysis forcing dataset<sup>48</sup> and therefore only differ in horizontal resolution and the  
372 associated diffusion scheme and coefficients.

373

374

375

376 **Observational constraints**

377 Observational sea surface density constraints were derived from the World Ocean Atlas 2013  
378 temperature and salinity climatologies<sup>25</sup>. The maximum Arctic Ocean sea surface density was  
379 then calculated in the same manner as for the ESM ensemble.

380 The uncertainty associated with Arctic Ocean maximum sea surface density observational  
381 constraints was estimated using standard propagation of uncertainty and combining (1) the  
382 published standard deviations of sea surface temperature and salinity for each grid cell and each  
383 month in WOA2013 to derive standard deviations for sea surface density, and (2) the standard  
384 deviation obtained when computing the weighted mean of 95<sup>th</sup> percentile density waters.

385 Arctic Ocean salinity in World Ocean Atlas 2013 was recently evaluated against available in-situ  
386 data<sup>49</sup>. This comparison suggests that salinity observations in the World Ocean Atlas may have a  
387 small negative bias in the Barents Sea that may contribute to a negative density bias.  
388 Corroboration and correction of such a bias would, if anything, result in a minor increase in our  
389 constrained estimates of projected Arctic Ocean anthropogenic carbon and associated  
390 acidification.

391

392 **Probability density functions of anthropogenic carbon and ocean acidification**

393 Probability density functions (PDFs) of anthropogenic carbon storage and basin-averaged  $\Omega_{\text{arag}}$ ,  
394  $\Omega_{\text{calc}}$  and pH in 2100 were calculated for the unconstrained (prior) CMIP5 ensemble and the  
395 emergent constraints. The prior PDF was derived assuming all models were equally likely and

396 sampled from a Gaussian distribution. The constrained PDFs were calculated as the normalised  
397 product of the conditional PDF of the emergent relationship and the PDF of the observational  
398 constraint following previously established methodologies<sup>21,22,50</sup>.

399

400

401 **References (Methods)**

- 402 41. Bates, N. R. & Mathis, J. T. The Arctic Ocean marine carbon cycle: Evaluation of air-sea  
403 CO<sub>2</sub> exchanges, ocean acidification impacts and potential feedbacks. *Biogeosciences* **6**, 2433–  
404 2459 (2009).
- 405 42. Tanhua, T. et al. Ventilation of the Arctic Ocean: mean ages and inventories of  
406 anthropogenic CO<sub>2</sub> and CFC-11. *J. Geophys. Res.* **114** (2009).
- 407 43. Orr, J. C. & Epitalon, J.-M. Improved routines to model the ocean carbonate system:  
408 mocsy 2.0. *Geosci. Model Dev.* **8**, 485–499 (2015).
- 409 44. Dickson, A. G., Sabine, C. L. & Christian, J. R. (eds) *Guide to Best Practices For Ocean CO<sub>2</sub>*  
410 *Measurements* 191 (PICES Special Publication 3, 2007).
- 411 45. Shu, Q., Song, Z. & Qiao, F. Assessment of sea ice simulations in the CMIP5 models.  
412 *Cryosphere* **9**, 399–409 (2015).
- 413 46. Shu, Q., Wang, Q., Su, J., Li, X., & Qiao, F. Assessment of the Atlantic water layer in the  
414 Arctic Ocean in CMIP5 climate models. *Clim. Dyn.* **53** 5279-5291 (2019).
- 415 47. Aumont, O. & Bopp, L. Globalizing results from ocean in situ iron fertilization studies. *Glob.*  
416 *Biogeochem. Cycles* **20**, GB2017 (2006).
- 417 48. Brodeau, L., Barnier, B., Treguier, A. M., Penduff, T. & Gulev, S. An ERA40-based  
418 atmospheric forcing for global ocean circulation models. *Ocean Model.* **31**, 88–104 (2010).
- 419 49. Xie, J., Raj, R. P., Bertino, L., Samuelsen, A., & Wakamatsu, T. Evaluation of Arctic Ocean  
420 surface salinities from SMOS and two CMEMS reanalyses against in situ data sets. *Ocean Sci.* **15**,

421 1191–1206 (2019).

422 50. Wenzel, S., Cox, P. M., Eyring, V. & Friedlingstein, P. Emergent constraints on climate-  
423 carbon cycle feedbacks in the CMIP5 Earth system models. *J. Geophys. Res. Biogeosciences* **119**,  
424 2013JG002591 (2014).

425

426

427

428 **Acknowledgements**

429 This study was funded by the H2020 C-CASCADES grant (ref 643052), the H2020 CRESCENDO  
430 grant (ref 641816), the H2020 4C grant (ref 821003), the Agence Nationale de la Recherche grant  
431 ANR-18-ERC2-0001-01 (CONVINCE), the MTES/FRB Acidoscope project and the ENS-Chanel  
432 research chair. We acknowledge the World Climate Research Programme's Working Group on  
433 Coupled Modelling, which is responsible for CMIP. For CMIP the US Department of Energy's  
434 Program for Climate Model Diagnosis and Intercomparison provided coordinating support and  
435 led the development of software infrastructure in partnership with the Global Organisation for  
436 Earth System Science Portals. The authors also thank the IPSL modelling group for the software  
437 infrastructure, which facilitated CMIP5 analysis, Jean-Marc Molines, Laurent Brodeau, and  
438 Bernard Barnier for developing the DRAKKAR ORCA05 and ORCA025 global configurations of  
439 NEMO and Jennifer Simeon, Christian Ethé, Marion Gehlen, and James C. Orr for the  
440 implementation of NEMO-PISCES within these configurations.

441

442 **Author contributions**

443 This study was conceived by all coauthors. J.T. performed the model output analysis and  
444 produced the figures, with help from L.K. and L.B. All authors contributed ideas, discussed the  
445 results and wrote the manuscript.

446

447

448 **Author information**

449 The authors declare no competing financial interests. Correspondence and requests for materials  
450 should be addressed to J.T (jens.terhaar@climate.unibe.ch).

451

452 **Data availability**

453 The Earth system model output used in this study is available via the Earth System Grid  
454 Federation (<https://esgf-node.ipsl.upmc.fr/projects/esgf-ipsl/>). Observations from the World  
455 Ocean Atlas 2013 (<https://www.nodc.noaa.gov/OC5/woa18/>) and GLODAPv2  
456 ([https://www.nodc.noaa.gov/ocads/oceans/GLODAPv2\\_2019/](https://www.nodc.noaa.gov/ocads/oceans/GLODAPv2_2019/)) are available via the National  
457 Oceanic and Atmospheric Administration. Prior to publication, the output of ocean-only NEMO-  
458 PISCES simulations is openly accessible on the ODATIS-supported center ‘Sea scientific open data  
459 publication’ (<https://doi.org/10.17882/72239>).

460

461 **Code availability**

462 The Python module ‘statsmodels’ (<https://www.statsmodels.org/stable/index.html>) was used for linear  
463 regression and the calculation of prediction intervals. The mocsy2.0 routines were used to calculate the  
464 ocean carbonate system variables (<http://ocmip5.ipsl.jussieu.fr/mocsy/>). The Climate Data Operators  
465 (CDO) were used for regridding of CMIP5 model output (<https://code.mpimet.mpg.de/projects/cdo/>). The  
466 code for the NEMO ocean model version 3.2 is available under CeCILL license online ([http://www.nemo-](http://www.nemo-ocean.eu)  
467 [ocean.eu](http://www.nemo-ocean.eu)).

468 **Extended Data:** Emergent constraint on Arctic

469 Ocean acidification in the twenty-first century

470 **Jens Terhaar<sup>1,2\*</sup>, Lester Kwiatkowski<sup>1,3</sup>, Laurent Bopp<sup>1</sup>**

471 <sup>1</sup> LMD/IPSL, Ecole Normale Supérieure/PSL Université, CNRS, Ecole Polytechnique, Sorbonne  
472 Université, Paris, France

473 <sup>2</sup> Oeschger Centre for Climate Change Research and Climate and Environmental Physics, Physics  
474 Institute, University of Bern, Bern, Switzerland

475 <sup>3</sup> LOCEAN, Sorbonne Université-CNRS-IRD-MNHN, Paris, France

476

477

478

479

480

481

482

483 **\*Jens Terhaar**

484 **Climate and Environmental Physics, Physics Institute**



485 University of Bern

486 Sidlerstrasse 5

487 3012 Bern

488 Switzerland

489 [jens.terhaar@climate.unibe.ch](mailto:jens.terhaar@climate.unibe.ch)

490 **Extended Data Table 1. The probability (%) of different year 2100 acidification extremes under RCP8.5**  
491 **in the CMIP5 prior and after the application of the maximum surface density emergent constraint.**

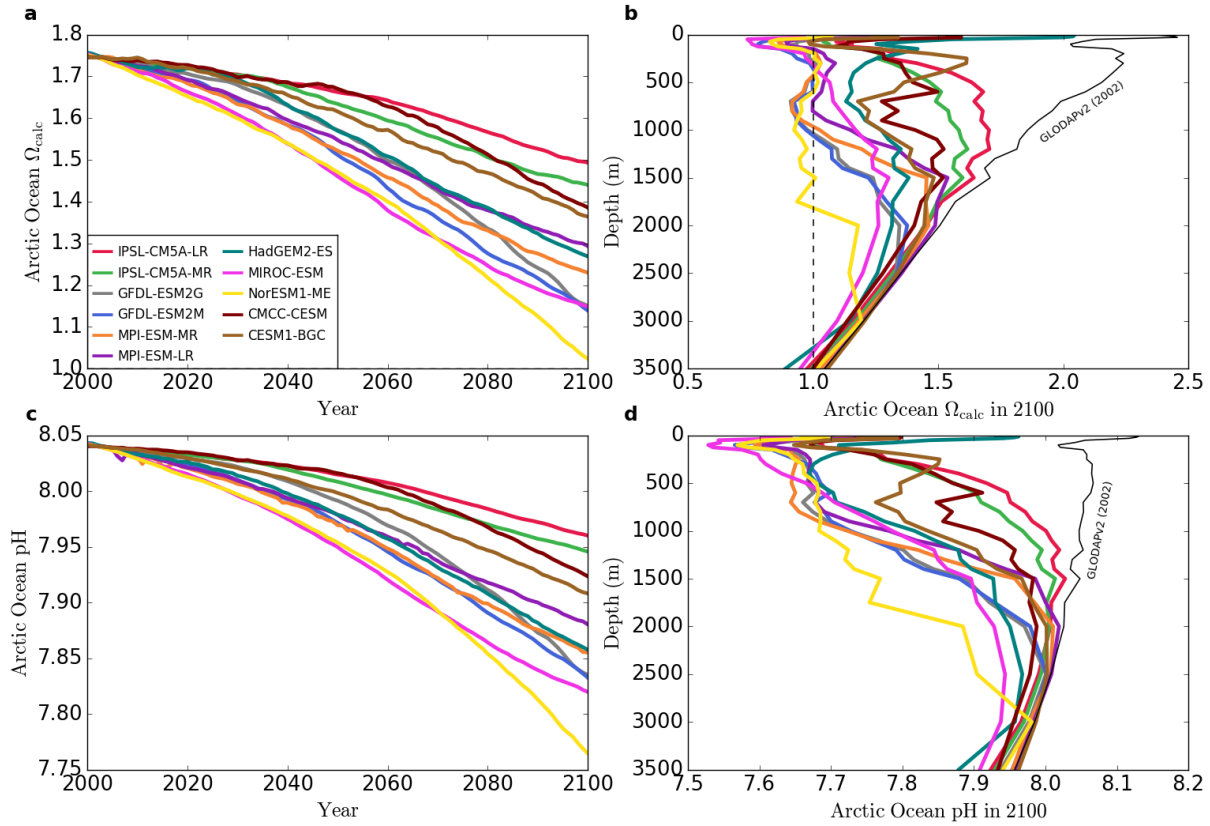
492

---

	$\Omega_{\text{arag}} < 0.75$		$\Omega_{\text{calc}} < 1.0$		pH < 7.85	
	Arctic Basin (0-bottom)	Mesopelagic (400-800m)	Arctic Basin (0-bottom)	Mesopelagic (400-800m)	Arctic Basin (0-bottom)	Mesopelagic (400-800m)
CMIP5 prior	24	51	3	23	35	83
Emergent constraint	41	88	1	37	62	100

---

493



494

495

496

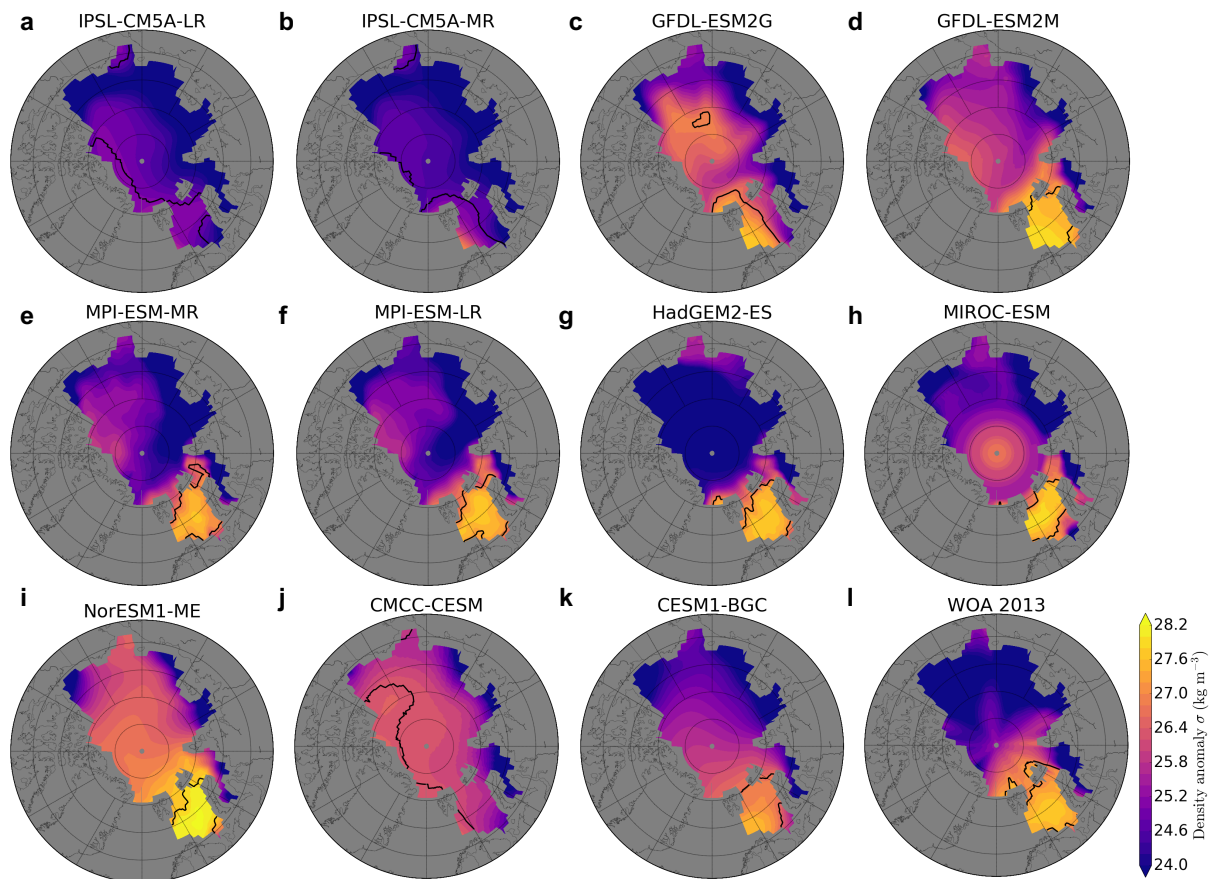
497 **Extended Data Figure 1. Projections of Arctic Ocean calcite saturation state and pH. a,** ESM

498 projections of the twenty-first century Arctic Ocean basin-averaged  $\Omega_{\text{calc}}$  and **c,** basin-averaged

499 pH. Vertical profiles of **b,** basin-averaged  $\Omega_{\text{calc}}$  and **d,** pH in 2100 for the 11 ESMs. The GLODAPv2

500 observational profiles of  $\Omega_{\text{calc}}$  and pH for 2002 are marked as a black line in **b** and **d**.

501



502

503

504 **Extended Data Figure 2. Arctic Ocean surface water density.** Present-day annual-mean sea  
 505 surface density from **a-k**, the 11 ESMs and from **l**, World Ocean Atlas 2013 observations. Contours  
 506 delineate regions that contribute to the maximum surface density as defined by the 95<sup>th</sup>  
 507 percentile densities.

508

509

510

511

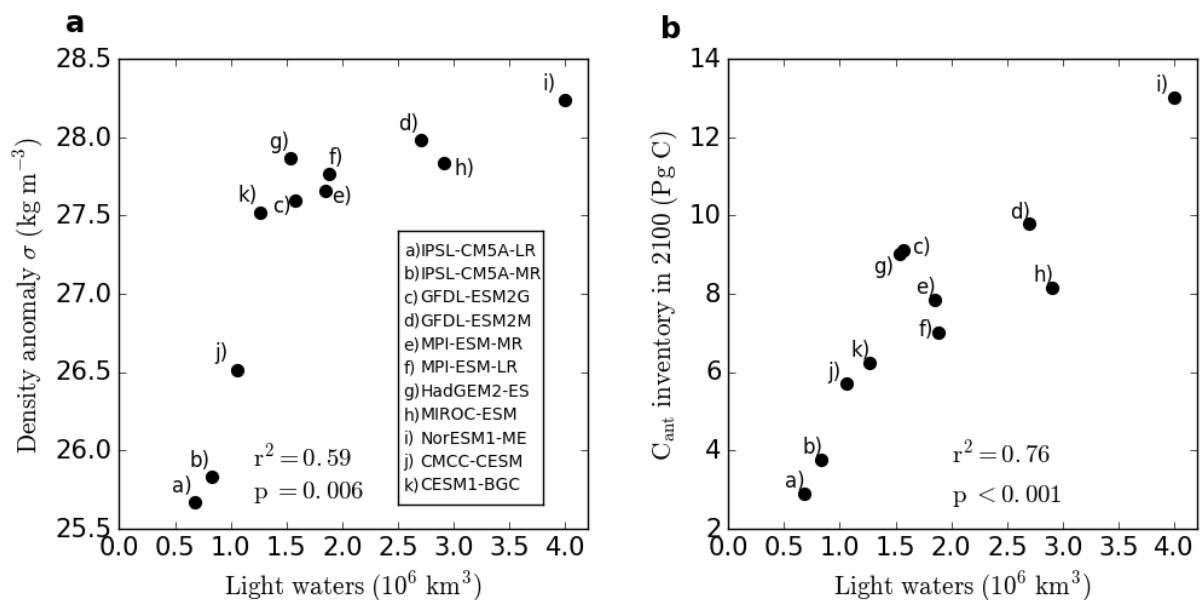
512

513

514

515

516  
 517  
 518  
 519  
 520  
 521  
 522  
 523  
 524  
 525  
 526  
 527  
 528  
 529  
 530



531

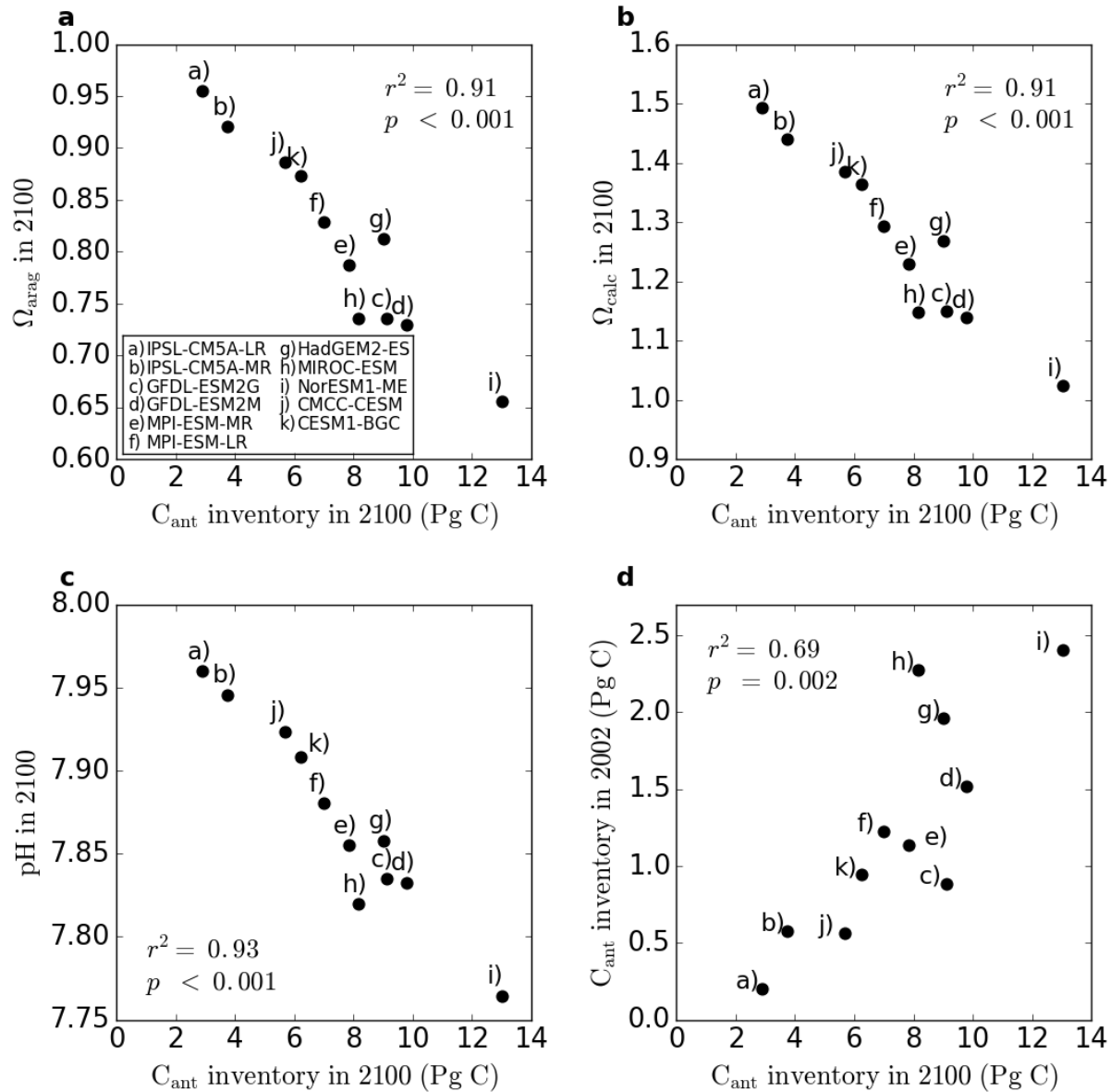
532

533 **Extended Data Figure 3. Arctic Ocean present-day density anomaly and anthropogenic carbon**

534 **inventory in 2100 against the volume of light waters: a, Arctic Ocean present-day maximum**

535 density anomaly and **b**, Arctic Ocean anthropogenic carbon inventory in 2100 against the volume  
536 of light waters. The volume of light waters is defined as the volume of water masses with  
537 densities below the respective maximum sea surface density (95<sup>th</sup> percentile waters).

538



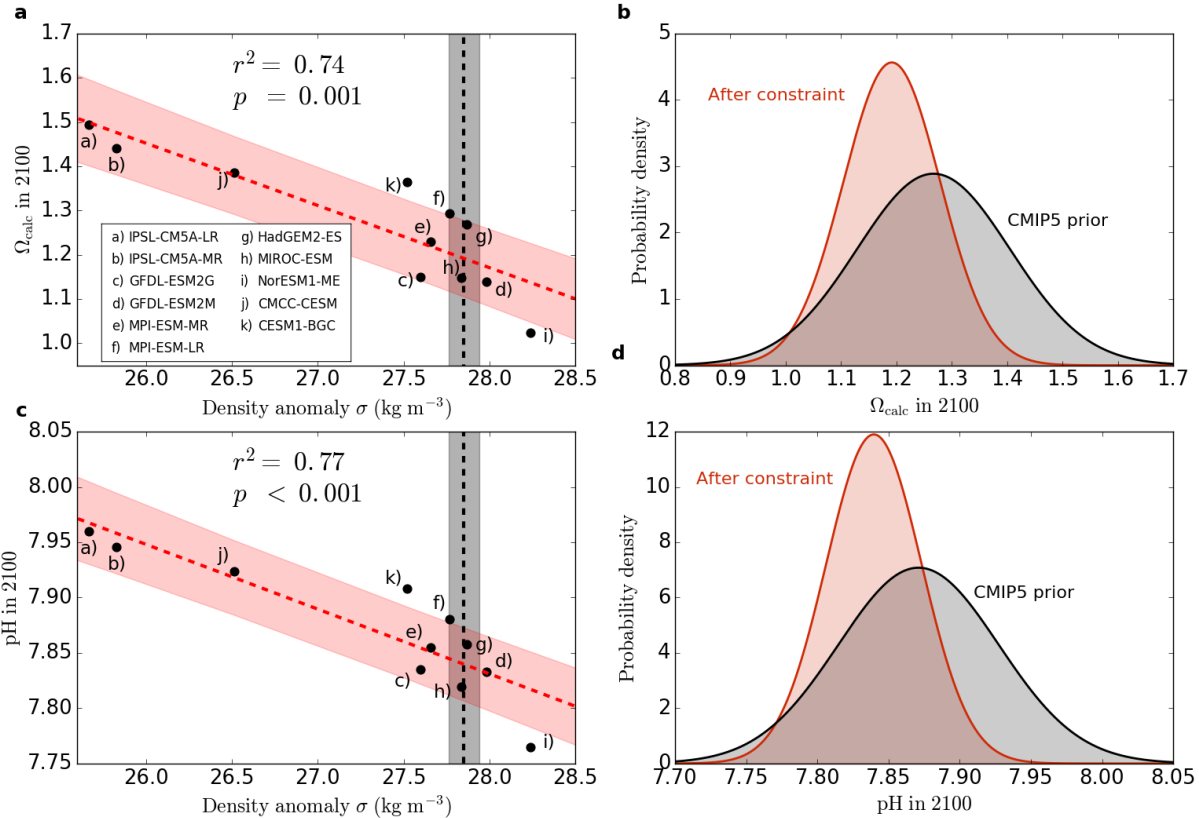
539

540

541 **Extended Data Figure 4. Correlations between projections of the Arctic Ocean anthropogenic**  
 542 **carbon inventory and  $\Omega_{\text{arag}}$ ,  $\Omega_{\text{calc}}$  and pH.** Arctic Ocean basin-averaged **a**,  $\Omega_{\text{arag}}$  in 2100, **b**,  $\Omega_{\text{calc}}$  in  
 543 2100, **c**, pH in 2100, and (d) the anthropogenic carbon inventory in 2002 against the  
 544 anthropogenic carbon inventory in 2100 for the 11 ESMs.

545

546



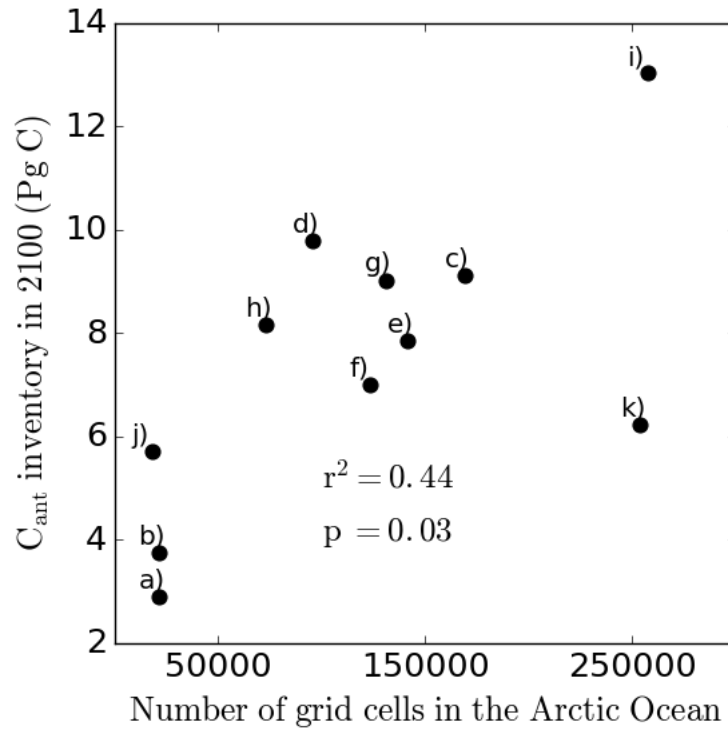
547

548

549

550 **Extended Data Figure 5. Emergent constraints on projected  $\Omega_{\text{calc}}$  and pH. a,** The projected Arctic  
 551 Ocean basin-averaged  $\Omega_{\text{calc}}$  and **c,** basin-averaged pH in 2100 against present-day maximum sea  
 552 surface density (95<sup>th</sup> percentile waters) for the ESM ensemble (black dots). Linear regression fits  
 553 (red dashed lines) and the associated 68 % prediction intervals are shown, as are data-based  
 554 estimates of present-day maximum sea surface density (black dashed lines) with the associated  
 555 standard deviation (black shaded area). Probability density functions for the end-of-century **b,**  
 556 Arctic Ocean basin-averaged  $\Omega_{\text{calc}}$  and **d,** basin-averaged pH, before (black) and after (red) the  
 557 emergent constraint is applied.

558



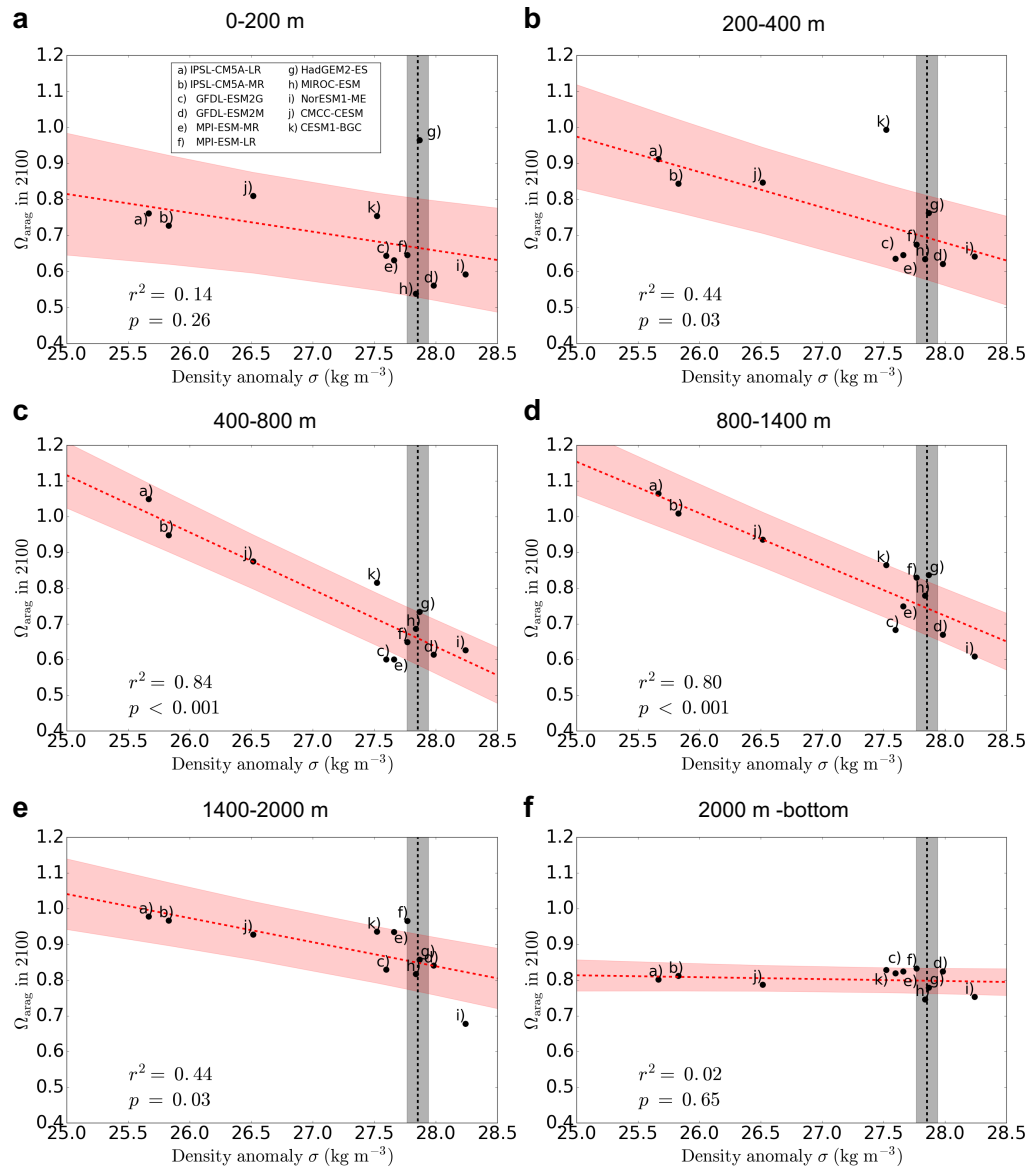
559

560

561 **Extended Data Figure 6. Arctic Ocean anthropogenic carbon inventory in 2100 against the**  
 562 **number of grid cells in the Arctic Ocean on the native model grid.** Arctic Ocean anthropogenic  
 563 carbon inventory in 2100 against number of grid cells on the native model grid in the Arctic Ocean  
 564 for each of the 11 ESMs.

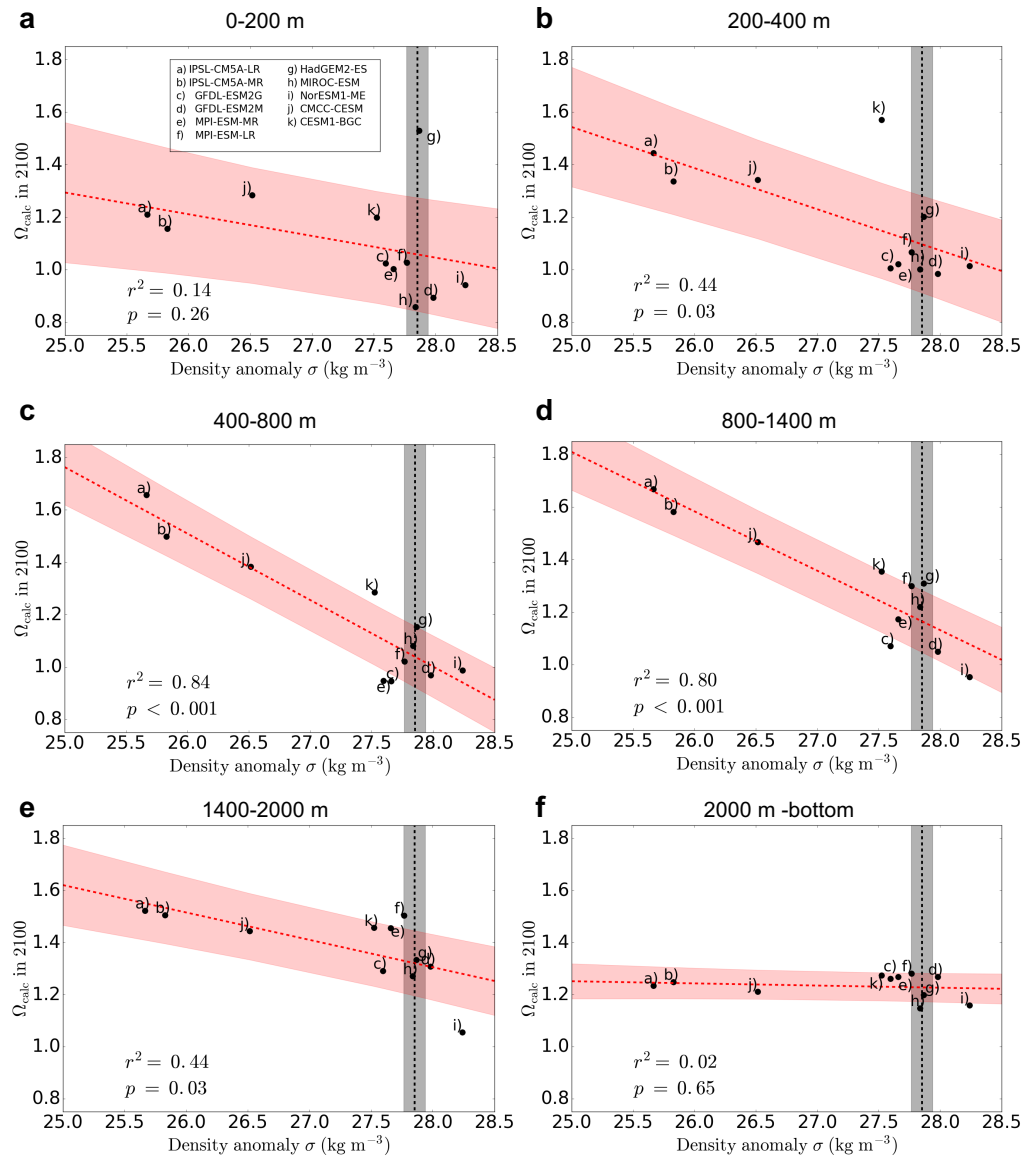
565





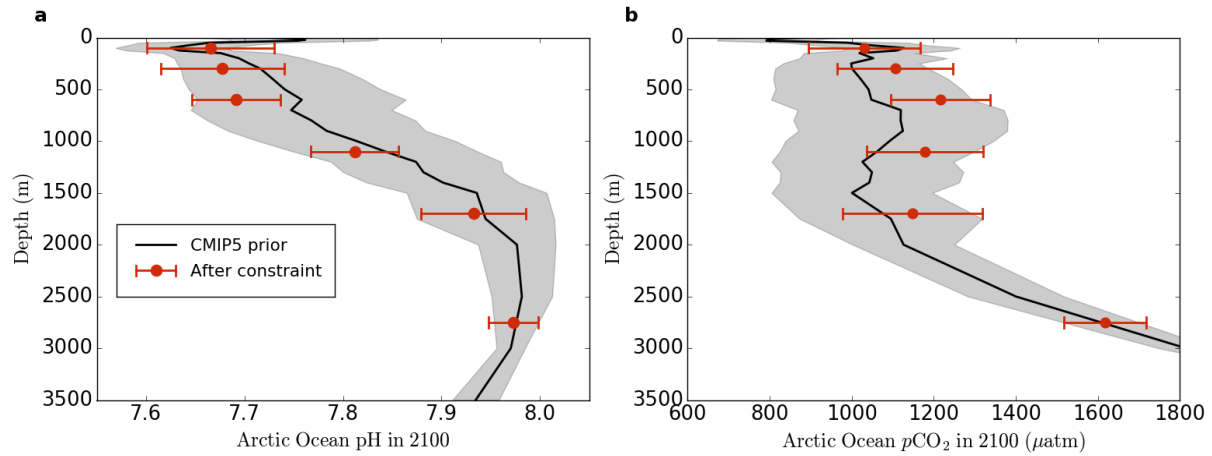
566

567 **Extended Data Figure 7. Emergent constraints on future aragonite saturation state in different**  
 568 **depth layers.** The projected end-of-century Arctic Ocean  $\Omega_{\text{arag}}$ , across six depth layers from a-f,  
 569 against maximum sea surface density (95<sup>th</sup> percentile waters) for the ESM ensemble (black dots).  
 570 Linear regression fits (red dashed lines) and the associated 68 % prediction intervals are shown,  
 571 as are data-based estimates of present-day maximum sea surface density (black dashed lines)  
 572 with the associated standard deviation (black shaded area).



573

574 **Extended Data Figure 8. Emergent constraints on future calcite saturation state in different**  
 575 **depth layers.** The projected end-of-century Arctic Ocean  $\Omega_{\text{calc}}$ , across six depth layers from **a-f**,  
 576 against maximum sea surface density (95<sup>th</sup> percentile waters) for the ESM ensemble (black dots).  
 577 Linear regression fits (red dashed lines) and the associated 68 % prediction intervals are shown,  
 578 as are data-based estimates of present-day maximum sea surface density (black dashed lines)  
 579 with the associated standard deviation (black shaded area).



580

581

582 **Extended Data Figure 9. Constrained end-of century Arctic Ocean vertical profiles of pH and**  
 583  **$p\text{CO}_2$ .** Multi-model mean vertical profiles of basin-averaged **a**, pH and **b**,  $p\text{CO}_2$  in 2100 (black lines)  
 584 with the associated standard deviation (grey shading). Constrained estimates of pH and  $p\text{CO}_2$   
 585 (red dots) are shown for six different depth layers (0-200 m, 200-400 m, 400-800 m, 800-1400 m,  
 586 1400-2000 m, 2000-3500 m). The constrained estimates are shown at the mid-point of each layer,  
 587 with error bars representing  $\pm$  one standard deviation.

588

589

590

591

592

593

594

595

596

597

598